

RSC Publishing Faraday Discussions

Impact of PEG additives and pore rim functionalization on water transport through sub-1-nm carbon nanotube porins

Journal:	<i>Faraday Discussions</i>
Manuscript ID	FD-ART-03-2018-000068
Article Type:	Paper
Date Submitted by the Author:	20-Mar-2018
Complete List of Authors:	Tunuguntla, Ramya; LLNL, Hu, Andrew; LLNL, Physics and Life Sciences Zhang, Yuliang; LLNL, Physics and Life Sciences Noy, Aleksandr; LLNL, Physics and Life Sciences

SCHOLARONE™
Manuscripts



ARTICLE

Impact of PEG additives and pore rim functionalization on water transport through sub-1-nm carbon nanotube porins

Ramya H. Tunuguntla,^{a,†} Andrew Y. Hu,^a Yuliang Zhang,^a and Aleksand Noy^{*,a,b}

Received 00th March 2018,
Accepted 00th January 20xx

DOI: 10.1039/x0xx00000x

www.rsc.org/

Carbon nanotubes represent one of the most interesting examples of a nanofluidic channel that combines extremely small diameters with atomically smooth walls and well-defined chemical functionalities at the pore entrance. In the past, sub-1-nm diameter carbon nanotube porins (CNTPs) embedded in a lipid membrane matrix demonstrated extremely high water permeabilities and strong ion selectivities. In this work, we explore additional factors that can influence transport in these channels. Specifically, we use stopped-flow transport measurements to focus on the effect of chemical modifications of the CNT rims and chaotropic polyethyleneglycol (PEG) additives on CNTP water permeability and Arrhenius activation energy barriers for water transport. We show that PEG, especially in its more chaotropic coiled configuration, enhances the water transport and reduces the associated activation energy. Removal of the static charges on the CNTP rim by converting -COOH groups to neutral methylamide groups also reduces the activation energy barriers and enhances water transport rates.

Introduction

Modern understanding of the physics of fluid flow is based on the Navier-Stokes equations that were developed by Claude-Louis Navier and George Stokes in the first part of the 19th century. Over the next two centuries this interpretation of fluid dynamics has proven surprisingly resilient and accurate over multiple length scales.¹ Yet, biologists and physicists realize that we are now starting to approach the limits of classical fluid dynamics as the dimensions of the fluidic channels start to approach molecular scale and enter the realm of nanofluidics.^{1, 2} Unique features of transport in biological pores, such as fast and selective water transport in aquaporins,³ have provided some of the earliest examples of these phenomena. Recent reports of fast transport in carbon nanotubes (CNTs),⁴⁻⁶ graphene-based membranes,⁷ and other nanofluidic systems show that these phenomena are not unique to biological systems, but instead represent a profound shift in the physics of fluid flow at the nanoscale.

Several major factors are responsible for the unusual flow enhancements at these scales. Strong molecular confinement can severely restrict or restructure interactions between fluid molecules, leading to unusual configurations, such as single-chain water.⁸ As the channel dimensions shrink, surface effects

gain prominence; for example, unusual slip conditions at the atomically smooth carbon nanotube walls are one of the key mechanisms enabling fast water transport through the CNT pores.⁹ Finally, as the dimensions of the pore shrink, solvent and solute interactions with the pore rim and channel functionality can play a major role in pore selectivity, as evidenced by structure of biological ion channels.¹⁰

We recently showed that a combination of molecular confinement and strong wall slip in narrow 0.8 nm diameter carbon nanotube porins (nCNTPs), short CNT channels embedded in a lipid membrane matrix, leads to high rates of the water transport that can exceed even those of aquaporins.⁶ We also observed that we can enhance the transport by introducing chaotropic additives to the feed water and by neutralizing the charges at the nanotube pore rim. In this work, we explore these phenomena further by studying the transport through nCNTPs in presence of several forms of polyethyleneglycol (PEG) additive. We also explore the effect of permanent chemical functionalization of the CNTP rim on the overall efficiency and energy barrier for water transport.

Results and discussion

Our previous measurements showed that 0.8 nm diameter CNTPs, which exhibit single-file water wire arrangement inside the channel, have water permeabilities 5.8 times greater than those of the biological gold standard, aquaporin 1 (AQP1).⁶ These measurements and the associated activation energy measurements from the temperature dependence of water flux identified several potential barriers to water transport. First, to enter the inner regions of the nCNTP channels, water

^a Physics and Life Sciences Directorate, Lawrence Livermore National Laboratory, Livermore, CA 94550

^b School of Natural Sciences, University of California Merced, Merced, CA 93454.

^c Correspondence to A.N.: noy1@llnl.gov

[†] Current address: PACT Pharma, Hayward, CA 94545

Electronic Supplementary Information (ESI) available: [details of any supplementary information available should be included here]. See DOI: 10.1039/x0xx00000x

molecules have to lose a significant number of hydrogen bonds that they form with surrounding water molecules. Another energy barrier component comes from the electrostatic interactions between the negatively-charged carboxylic acid (COO^-) groups on the nCNTP rim and water molecules that pass through this pore region.

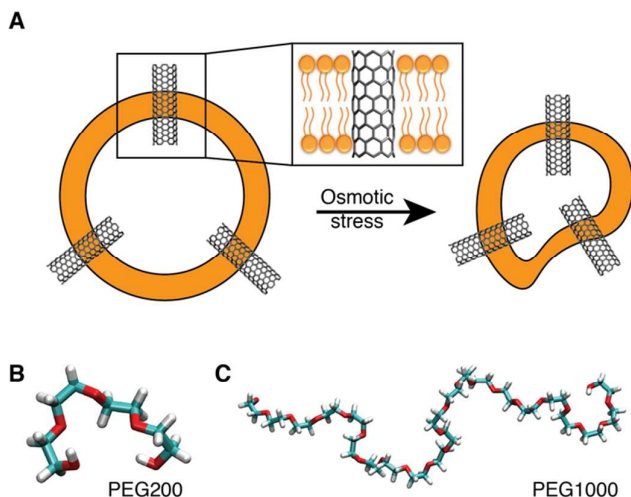


Figure 1. A. Schematic of the osmotically-driven water transport experiments. Under the pressure of an external osmolyte, water escapes from the liposomes through the carbon nanotube porins, leading to liposome shrinkage. B. 3D representation of a PEG₂₀₀ molecule obtained from MD simulations. C. 3D representation of a PEG₁₀₀₀ molecule showing coiled structure.

Our past work also highlighted the role of intermolecular hydrogen bonding in the water transport process by showing that water flux can be modified by kosmotropic and chaotropic additives that affect the structure of water. To explore this phenomenon further we have studied water transport through nCNTPs in presence of two different forms of chaotropic PEG (Fig. 1). Specifically, we chose two PEG oligomers, PEG₂₀₀ and PEG₁₀₀₀, because they represent two different PEG configurations with different levels of chaotropic activity. The shorter PEG₂₀₀ molecule has a small 1.8 nm hydrated diameter and a compact structure (Fig. 1B). A longer PEG₁₀₀₀ molecule has a larger 9 nm hydrated diameter and forms a coiled structure in solution (Fig. 1C). The combination of larger size and the solvated structure of the PEG₁₀₀₀ makes it a stronger chaotrope.¹¹

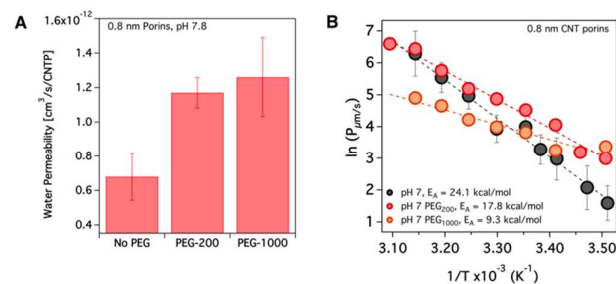


Figure 2. A. Unitary water permeability of 0.8 nm diameter CNTPs measured in the osmotically-driven transport experiments in presence of different PEG additives. B. Temperature dependence of the overall water permeability of

CNTP-LUVs measured in presence of different PEG additives. Dashed lines correspond to Arrhenius fits to the data.

To focus on the chaotropic activity, we compared the effect of adding 30 mM of PEG₁₀₀₀ and 150mM of PEG₂₀₀ because these concentrations kept the relative amount of PEG in the sample constant. As expected, the presence of both types of PEG additives resulted in the enhanced water transport through CNTPs, where in both cases the unitary water permeability was increased by approximately 1.7 times (Fig. 2A). In contrast, the measurements of the Arrhenius activation energy for the transport revealed drastic differences. Addition of short uncoiled PEG₂₀₀ to the solution inside the vesicles (i.e. on the upstream side) resulted in the drop of the activation energy value from 24.1 kcal/mol to 17.8 kcal/mol (Fig. 2B). In contrast, a control experiment where PEG₂₀₀ was added to the outside (downstream side) solution, showed no changes in the activation energy value (data not shown), arguing that chaotropic additives primarily influence the process of water entry into the CNTP pores. Furthermore, when we added the longer coiled chain PEG₁₀₀₀ to the upstream side, the activation energy value dropped even further to 9.3 kcal/mol (Fig. 2B). The larger drop in the activation energy recorded with PEG₁₀₀₀ is consistent with the higher chaotropic activity of this compound.

Also, it was striking that a rather large drop in the activation energy did not produce corresponding changes in the unitary water permeability; this result argues that the relationship between permeability and activation energy barriers for carbon nanotubes is significantly more complicated than that of aquaporins.¹²

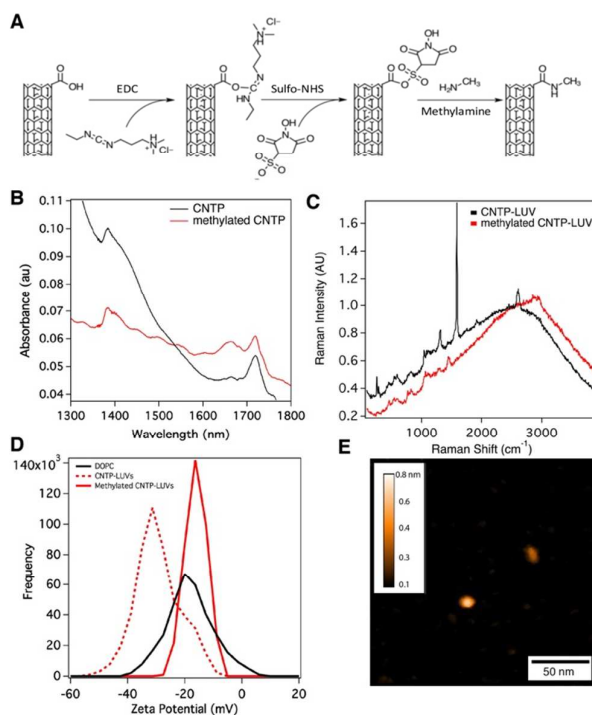


Figure 3. A. Schematics of the functionalization of the CNTP rim with methylamide groups. B. Near-IR absorption spectra of the unfunctionalized (black line) and functionalized (red line) CNTPs. C. Raman spectra of lipid vesicles containing functionalized (red line) and unfunctionalized (black line) CNTPs. D. Histograms of the ζ -potential value measured for DOPC lipid vesicles (black line)

and vesicles containing functionalized (solid red line) and unfunctionalized (dashed red line) CNTPs. E. Frame from HS-AFM movie (see Suppl. Mater. for the full movie) showing two CNTPs embedded in the supported lipid bilayer on mica surface.

Our previous measurements indicated that the barrier for water entry into the CNTPs can be reduced by removing negative charge at the pore entrance by acidifying the aqueous solution. To study this phenomenon further and to exclude the possibility of pH change influencing the water transport mechanism inside the pore we used chemical modification to convert COOH groups at the CNTP rim to uncharged methylamide groups. We used carbodiimide (EDC) coupling chemistry (Fig. 3A), which has been used previously for site-specific modification of carbon nanotube rims. In this process COOH groups are first converted into a sulfo-NHS ester and then reacted with methylamine to produce the final methylamide group product. To ensure that both rims of the CNTPs were modified we performed the chemical modification before incorporating the CNTPs into the lipid vesicles (see Experimental section for details).

Near-IR absorption spectra of the reaction products show clear evidence of absorption peaks at around 1385 nm and 1720 nm that correspond to S_{11} transition states, indicating that the carbon nanotube structure was preserved during chemical modification. However, the relative intensity of the signal is diminished, indicating that functionalization process and subsequent purification resulted in a significant loss of CNTPs. Comparison of the Raman spectra of the lipid vesicles made with the unfunctionalized CNTPs with that of vesicles made with the functionalized CNTPs (MeCNTPs) also shows evidence of material loss: the signature G and G' Raman bands of CNTPs are still present, but their intensity is sharply reduced (Fig. 3C). We can use the comparison of the intensity of the CNTP Raman peaks with the broad lipid Raman band¹³ to quantify this loss; indeed, the relative intensity of the G -band signal indicates that the vesicles made with MeCNTPs contain ca. 8.9 times less nanotube material. We speculate that this factor reflects the aggregate effect of the material loss during functionalization and a reduced propensity of the MeCNTPs to incorporate into the lipid bilayers due to the reduced polarity of the CNTP region near the rim.

High-speed AFM (HS-AFM) imaging of the CNTPs in the supported lipid bilayers obtained by fusing MeCNTP-LUVs onto a mica support surface (Fig. 3E) also supports these conclusions. Previous work indicated that HS-AFM is capable of visualizing rapidly-diffusing unmodified CNTPs in supported lipid bilayers. As is the case with bilayers containing unfunctionalized CNTPs, HS-AFM images of MeCNTPs in supported lipid bilayers show distinct sharp features indicating that even after neutralization the MeCNTPs do not fully embed into the hydrophobic bilayer domain; instead, they still protrude above the lipid layer plane. This behaviour indicates that the interactions of the carbon nanotube sidewalls with the lipid tails, as well as the tail-tail interactions dominate the energetics of CNT embedding in the lipid bilayers. This observation also supports the conclusion that the ends of MeCNTPs are not buried within the bilayer and remain accessible for transport. The average area density of the

MeCNTPs obtained from the HS-AFM data, 6 porins/LUV, AFM images also agrees with the density estimate, 5 porins/LUV based on the Raman data. Interestingly, MeCNTPs show slower lateral diffusion in supported lipid bilayers (see Suppl. Materials) than unmodified CNTPs, indicating stronger interactions of the terminal methylamide groups with the mica support surface.

ξ -potential measurements of the vesicles containing MeCNTPs (Fig. 3D) also indicate a reduced surface charge density after CNTP rim functionalization. Incorporation of the unmodified CNTPs in DOPC liposomes changes the ξ -potential value of the liposomes from -17.2 mV to -29.3 mV, which is consistent with the negative charge on the COO⁻-terminated CNTPs. When unmodified CNTPs are replaced with MeCNTPs, the value of the ξ -potential drops to -15.8 mV, which is very close to the value obtained with pure DOPC vesicles, again confirming that functionalization converts the CNTP rims into an uncharged state.

Osmotically-driven water transport measurements through MeCNTPs embedded in DOPC vesicles indicated that functionalization has a strong effect on water permeability (Fig. 4). The unitary permeability of MeCNTPs ($1.2 \cdot 10^{-12}$ cm³/s/CNTP) increased about 6 times relative to that of the unfunctionalized CNTPs (Fig 4A). Moreover, this value is very close to the value that we previously measured for CNTPs at pH 3 ($1.0 \cdot 10^{-12}$ cm³/s/CNTP), indicating that the charge state of the nanotube rim indeed has a strong influence on the water permeability of CNTPs. Activation energy measurements (Fig. 4B) provide further corroboration for these conclusions. The Arrhenius factor measured for water transport through MeCNTPs (10.8 kcal/mol) is virtually identical to the value of 10.6 kcal/mol obtained for water transport through unmodified CNTPs at pH 3.

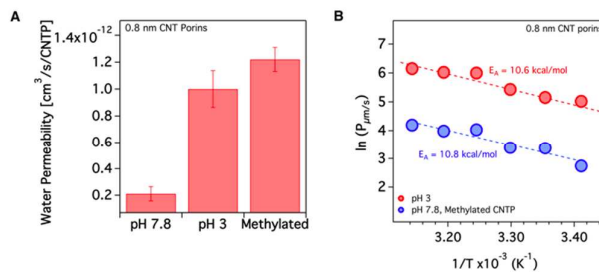


Figure 4. A. A. Unitary water permeability of unfunctionalized CNTPs measured at pH 3 and pH 7 compared to the water permeability of MeCNTPs measured at pH 7. B. Temperature dependence of the overall water permeability of vesicles containing unfunctionalized CNTPs measured at pH 3 and vesicles containing MeCNTPs measured at pH 7. Dashed lines correspond to Arrhenius fits to the data with corresponding activation energy values indicated on the graph.

These results provide some clues to the mechanism of water transport through carbon nanotube pores. We speculate that the presence of polar or charged functional groups on the CNTP rims benefits water entry into the nanotube by facilitating hydrogen bonding rearrangement required to transition from the bulk pattern to a water wire pattern in the pore interior. However, we speculate that interactions with the charged groups on the unmodified CNTP rims at neutral pH

may be too strong and can cause water molecules to pause at the entrance, slowing down the overall transport rate. Substituting these charges for uncharged yet still polar methylamide groups reduces the interactions and the corresponding energy barrier enough to eliminate this additional pause and speed up the overall transport rate.

Experimental

Liposome preparation and CNTP incorporation

1,2-dioleoyl-sn-glycero-3-phosphocholine (DOPC) lipid in chloroform was aliquoted (2 mg) into glass vials and the solvent was evaporated under a stream of air, then further dried overnight in a vacuum desiccator chamber. Liposomes were prepared by adding 1 mL of a 10 mM HEPES, pH 7.8 buffer to the dried lipid film to obtain a final lipid concentration of 2 mg/mL. For experiments that included kosmotropic PEG₄ or PEG₁₀₀₀, liposome samples were made with buffer that included those additives at the appropriate concentrations. To incorporate CNTPs into the liposomes, we first dried 2 mL of the appropriate CNTP solution overnight in a vacuum desiccator to remove the solvent. Dried CNTP film was hydrated with 1 mL of buffer and bath-sonicated for 30 seconds to ensure the nanotubes were completely solubilized and detached from the glass vial. This solution was subsequently used to hydrate a 2mg DOPC lipid film and further bath-sonicated for 30 seconds. The resulting liposome solution was hydrated at room temperature for 30 minutes. To ensure formation of large unilamellar vesicles (LUVs) or CNTP-LUVs, the samples underwent 10 cycles of freeze-thaw treatment wherein the liposomes were flash-frozen in liquid nitrogen and subsequently thawed at 50°C. The liposome samples were then extruded 21 times through a 200 nm pore-sized polycarbonate membrane using a mini-extruder (Avanti Polar Lipids). To separate free, unincorporated porins from the CNTP-liposome solution, we performed size exclusion chromatography with a column containing Sepharose CL-6B agarose (Sigma-Aldrich, St. Louis, MO), and collected fractions using 10 mM HEPES pH 7.8 buffer as an eluent. Fractions containing liposomes were pooled and stored for use in water permeability experiments.

Chemical modification of CNTp with Methylamine

CNTP stock solution¹⁴ was centrifuged at 15,000 x g for 20 minutes and supernatant was transferred into a clean 20 mL glass scintillation vial. The vial was placed in a desiccator to evaporate the solution and to form a dry film. 0.8 mg of 1-ethyl-3-(3-dimethylaminopropyl) carbodiimide (EDC) was added to 2 mL of BupH MES buffered saline (0.1M 2-(N-morpholino)ethanesulfonic acid (MES), 0.9% NaCl, pH 4.7) and mixed well. CNTP film was hydrated with 1 mL of the EDC solution and bath-sonicated for 60 seconds. 1.1 mg of N-hydroxysulfosuccinimide (Sulfo-NHS) was then added into 22 µL of MES buffer in a glass vial, then CNTP solution was added into the Sulfo-NHS solution, mixed well, and incubated at room temperature for 15 minutes. To stop the EDC/Sulfo-NHS reaction, we performed buffer exchange by adding the CNTP

solution into the 500 µL of buffer centrifuging it in a 3 kDa spin filter (Pierce), pre-hydrated with 10 mM HEPES buffer, pH 7.4, at 15,000×g for 20 minutes at room temperature. Supernatant was transferred (without disturbing the pellet) into a new hydrated spin filter and enough 10 mM HEPES buffer was added to achieve 500 µL volume, and the solution was centrifuged again at 15,000×g for 20 minutes. This step was repeated twice to thoroughly wash the solution and remove all unreacted reagents from the CNTP solution. To functionalize the porins with methylamine, stock methylamine solution was diluted using a series of steps with 10 mM HEPES buffer to achieve approximately 1000-fold excess over the amount required to functionalize CNTPs, then mixed with CNTP stock solution and buffer to achieve 1 mL final volume. This solution was then incubated for 4 hours at room temperature and then reactants were removed by 4-6 steps of buffer exchange (similar to those described for the previous washing steps). Methylamide functionalized CNTPs were stored in a glass vial.

Zeta potential measurements

Average liposome diameters were determined by dynamic light scattering (DLS) using a Zetasizer Nano-ZS90 (Malvern Instruments). Typically, 70 µL of the liposome sample was added to a disposable small volume cuvette (BRAND GmbH & Co. KG) and light scattering intensity of the liposomes was measured. Each size reading was obtained from an average of 10 individual measurements. The Zetasizer instrument was also used to measure the zeta potential as an indirect measure of surface charge density. For those measurements, 1 mL of a sample was loaded into a disposable folded capillary zeta cell and zeta potential measurements were recorded from an average of 100 readings per sample.

Raman and NIR spectroscopy of CNTPs

The Raman spectra were measured using a micro-Raman spectrometer (Nicolet Omega XR, Thermo Scientific) at laser wavelengths of 633 nm and 473 nm. The laser power was kept below 100 W/cm² for the study of CNT porins to avoid heating the samples. To prepare the samples for Raman analysis, equal aliquots of aqueous dispersions of the CNTP batches were dried on glass slides in a vacuum desiccator for 3-4 hours to form a greasy film spot on the slide and subsequently measured in the Raman spectrometer. To prepare solutions for NIR spectroscopy, CNTPs were dried and re-dissolved in 1% SDS in D₂O and then bath-sonicated for 30 seconds prior to the measurement.

CNT porin water permeability measurements

Water permeabilities of CNT porins or pure liposomes were measured using a stopped-flow instrument (SFM2000, BioLogic). The liposome samples were rapidly mixed with a hypertonic solution that caused them to shrink due to the osmotic gradient driving a water efflux. The osmolarity of each buffer was experimentally measured on a freezing-point osmometer (Osmomat 3000, Gonotec) to ensure accurate calculation of

permeabilities. Under these experimental conditions, a reduction in liposome volume led to an increase in the light scattering signal.¹⁵ Light scattering data were recorded at 594 nm, a 90° scattering angle, with an acquisition interval between 50–200 μs, and a measured dead time of 0.7 ms. For each osmolyte mixture, the light-scatter curve analysis was derived from an average of 5–8 individual runs. The analysis was performed as described previously.⁶ Briefly, the osmotic water permeability, p_f , in units of cm/s was calculated using the following expression:

$$p_f = \frac{k}{\left\{ \frac{SA}{V_0} (V_w)(C_{out} - C_{in}) \right\}} \quad [1]$$

where $k = -(\Delta V/V_0)/t$ is the shrinkage rate determined from single or double exponential fits to the light scattering data for LUVs or CNTP-LUVs, respectively; the inherent assumption for this approach is that change in intensity of the scattered light is proportional to the change in the vesicle volume ($\Delta V/V_0$). SA/V_0 is the liposome surface area to initial volume ratio, V_w is the partial molar volume of water (18 cm³), and $(C_{out} - C_{in})$ is the difference in osmolarity between the intravesicular and extravesicular aqueous solutions. For CNTP-LUVs the stopped flow scattering curves were fit to a double exponential function with two shrinkage rates. CNTP single-channel unit water permeability, P , with units of cm³/s, was calculated as the difference in permeability, between CNTP-LUVs and LUVs under the same osmotic gradient, multiplied the surface area of the CNT-LUV (SA), and divided by the number of porins incorporated in a 200 liposome for a given batch of CNT porins, incorporation efficiency ($I.E.$):

$$P_U = (p_{CNT-LUV} - p_{LUV}) * \frac{SA}{I.E.} \quad [2]$$

Activation energy measurements

Osmotically-driven water transport measurements were repeated for LUVs and CNTP-LUVs at temperatures between 10 and 50 °C. For the determination of the activation energy, the bulk permeability rates through CNTPs alone (with background liposomal permeability deducted), measured at varying temperatures were used to construct an Arrhenius plot. The slope of the plot was determined by linear regression.

High-speed AFM imaging.

The procedure is adopted from our previous work.¹⁶ Briefly, a small aliquote (4 μL) of liposome solution was deposited on the freshly cleaved mica surface and incubated for two hours at room temperature. Afterwards, the unfused liposomes were rinsed away with 20 μL of 10 mM HEPES (pH 7.8) for 5 times.

CNTP images were acquired in tapping mode at room temperature using a HS-AFM instrument (RIBM, Japan). The fluid cell was filled with 120 μL of 10mM HEPES buffer. The ultra-short AFM cantilevers with high density carbon/diamond like carbon (HDC/DLC) tips (USC-F1.2-k0.15, tip radius < 10 nm) were purchased from NanoWorld. In

addition, the dynamic proportional-integral-differential (PID) controller was used to reduce the probe “parachuting” artefacts from images. Images were typically collected from a 200 nm × 200 nm area at 128×128-pixel image size. The scan rate was 2 frames per second. Raw image sequences were converted to ImageJ stacks (W. Rasband, National Institutes of Health, Bethesda, MD) using custom software built with Matlab2015 (MathWorks, Natick, MA).

MD simulations of PEG structure.

PEG 200 and PEG 1000 models were obtained from all-atom molecular dynamics (MD) simulations using NAMD 2.10¹⁷ with CHARMM36 force field.¹⁸ The linear initial PEG 200 and PEG 1000 structures were solvated in tip3¹⁹ water spheres (radii of 7.98 nm and 39.31 nm respectively) with non-periodic boundary conditions. After 1000 steps of energy minimization, the PEG systems were equilibrated for 1 ns. Snapshots of the relaxed configuration of PEG 200 and PEG 1000 were taken from the last frame of the simulation.

Conclusions

These experiments highlight the importance of the entrance effects for transport through very small diameter nanopores. The same factors that enable high rates of transport through the narrow diameter carbon nanotube pores—molecular level confinement and smooth slippery walls—also amplify the importance of the hydrogen bonding rearrangement that has to occur for water molecules to enter the carbon nanotube pores. We showed that the energy barriers that arise from this rearrangement can be manipulated by either changing the electrostatic interactions using chemical modification of the pore entrance, or by adding chaotropic compounds to the feed water. Even though the degree of chaotropic activity generally correlates with water permeability, the relationship between the transport efficiency and measured energy barriers appears to be complicated and would require additional studies. Overall, our results provide additional clues for establishing the design rules for the next generation of carbon nanotube membranes for water purification. We believe that careful optimization of the pore structure, perhaps even mimicking the structures that biological channels use to mediate entrance into the pores, would help to realize the significant potential benefits of carbon nanotube membranes for water treatment applications.

Conflicts of interest

There are no conflicts to declare.

Acknowledgements

This work was supported by the US Department of Energy, Office of Basic Energy Sciences, Division of Materials Sciences and Engineering. Work at LLNL was performed under the auspices of the US Department of Energy under contract DE-AC52-07NA27344. Work at the Molecular Foundry at LBL was

supported by the Office of Science, Office of Basic Energy Sciences, of the US Department of Energy under contract DE-AC02-05CH11231.

Notes and references

1. L. Bocquet and E. Charlaix, *Chem. Soc. Rev.*, 2010, **39**, 1073-1095.
2. R. B. Schoch, J. Han and P. Renaud, *Rev. Mod. Phys.*, 2008, **80**, 839.
3. P. Agre, M. Bonhivers and M. J. Borgnia, *J. Biol. Chem.*, 1998, **273**, 14659-14662.
4. M. Majumder, N. Chopra, R. Andrews and B. J. Hinds, *Nature*, 2005, **438**, 44-44.
5. J. K. Holt, H. G. Park, Y. Wang, M. Stadermann, A. B. Artyukhin, C. P. Grigoropoulos, A. Noy and O. Bakajin, *Science*, 2006, **312**, 1034-1037.
6. R. Tunuguntla, R. Henley, Y.-C. Yao, T. A. Pham, M. Wanunu and A. Noy, *Science*, 2017, **357**, 792-796.
7. R. Nair, H. Wu, P. Jayaram, I. Grigorieva and A. Geim, *Science*, 2012, **335**, 442-444.
8. G. Hummer, J. C. Rasaiah and J. P. Noworyta, *Nature*, 2001, **414**, 188-190.
9. E. Secchi, S. Marbach, A. Niguès, D. Stein, A. Siria and L. Bocquet, *Nature*, 2016, **537**, 210-213.
10. D. A. Doyle, J. M. Cabral, R. A. Pfuetzner, A. Kuo, J. M. Gulbis, S. L. Cohen, B. T. Chait and R. MacKinnon, *Science*, 1998, **280**, 69-77.
11. L. Huang and K. Nishinari, *J. Polym. Sci. B.*, 2001, **39**, 496-506.
12. A. Horner, F. Zoicher, J. Preiner, N. Ollinger, C. Siligan, S. A. Akimov and P. Pohl, *Science Adv.*, 2015, **1**, e1400083.
13. R. H. Tunuguntla, X. Chen, A. Belliveau, F. I. Allen and A. Noy, *J. Phys. Chem.*, 2017, **121**, 3117-3125.
14. A. E. R. H. Tunuguntla, V. Frolov, A. Noy, *Nature Protoc.*, 2016, **11**, 2029-2047.
15. P. Latimer and B. E. Pyle, *Biophys. J.*, 1972, **12**, 764-773.
16. Y. Zhang, R. H. Tunuguntla, P.-O. Choi and A. Noy, *Phil. Trans. R. Soc. B.*, 2017, **372**, 20160226.
17. J. C. Phillips, R. Braun, W. Wang, J. Gumbart, E. Tajkhorshid, E. Villa, C. Chipot, R. D. Skeel, L. Kale and K. Schulten, *J. Comput. Chem.*, 2005, **26**, 1781-1802.
18. J. B. Klauda, R. M. Venable, J. A. Freites, J. W. O'Connor, D. J. Tobias, C. Mondragon-Ramirez, I. Vorobyov, A. D. Mackerell Jr and R. W. Pastor, *J. Phys. Chem. B.*, 2010, **114**, 7830-7843.
19. W. L. Jorgensen, J. Chandrasekhar, J. D. Madura, R. W. Impey and M. L. Klein, *J. Chem. Phys.*, 1983, **79**, 926-935.